Inorganic Chemistry Communications xxx (xxxx) 110877

Contents lists available at ScienceDirect

Inorganic Chemistry Communications

journal homepage: www.elsevier.com/locate/inoche

Short communication

A novel biogenic method to synthesis a ternary (ZnO-Ag)/g-C_3N_4 nanocomposite with an enhanced photocatalytic and antibacterial activities

M. MuthuKathija [a], R.M. Muthukrishnan [b], D. Renuka Devee [c], S.M. Abdul Kader [b], V. Rama [d], M. Sheik Muhideen Badhusha [a,*]

[a] Research Department of Chemistry, Sadakathullah Appa College (Autonomous), Affiliated to Manonmaniam Sundaranar University, Tirunelveli, Tamil Nadu, India
[b] Research Department of physics, Sadakathullah Appa College (Autonomous), Affiliated to Manonmaniam Sundaranar University, Tirunelveli, Tamil Nadu, India
[c] Research Department of Physics, Pachaiyappa's College (Autonomous), Affiliated to Madras University, Chennai, Tamil Nadu, India
[d] Research Department of Chemistry, Sarah Tucker College (Autonomous), Affiliated to Manonmaniam Sundaranar University, Tirunelveli, Tamil Nadu, Tirunelveli, India

ARTICLE INFO

Keywords:
(ZnO-Ag)/g-C_3N_4 nanocomposite
Photocatalytic activity
Antibacterial activity
Green route

ABSTRACT

One of the most effective ways to obtain high-efficiency photocatalysts is to create heterojunctions between two semiconductors with matched band structures. As a pioneering photocatalytic system, the S-scheme heterojunction system has demonstrated considerable promise in simplifying the separation and transfer of photogenerated carriers as well as developing high photoredox capacity. Hence, we report a novel biogenic method to synthesise ternary (ZnO-Ag)/g-C_3N_4 S-scheme nanocomposites via Terminalia Arjuna leaf extract as an effective reducing and capping agent. The X-ray diffraction technique gives the structural confirmation of well-crystalline Ag, g-C_3N_4, and ZnO nanoparticles, indicating the excellent reducing property of *Terminalia* Arjuna leaf extract. UV–Vis spectroscopy reveals the enhanced optical behaviour of (ZnO-Ag)/g-C_3N_4 by means of a reduction in their bandgap values, which would reflect in the photocatalytic performance of the material. The presence of secondary meltabilities such as phenolic compounds, alkaloids, terpenoids, and proteins in leaf extract employed in the nucleation and stability of (ZnO-Ag)/g-C_3N_4 nanocomposites was analysed using FTIR spectroscopy. XPS rules out the presence of any other secondary elements(impurity). The incorporation of silver metal in ZnO nanomaterials was investigated using TEM analysis. Finally, the photocatalytic activity and antibacterial activity of (ZnO-Ag)/g-C_3N_4 nanocomposites were compared with the pristine Ag-ZnO, g-C_3N_4, and ZnO nanoparticles.

1. Introduction

Hazardous chemicals and toxic water pollutants are the root causes of dangerous environmental issues that are receiving a great deal of attention among researchers. The textile and food industries use non-biodegradable organic dyes that pollute the environment, are extremely poisonous to flora and fauna, and have mutagenic effects on humans. Methylene blue and methyl orange are harmful chemicals that are primarily used as dyes in a variety of commercial applications such as textiles, papers, leathers, additives, laser printing, and so on. Because of their high surface area, porous structure, and crystalline nature, nanomaterials are the most effective and alternative material for removing toxic organic dye molecules from industrial waste water. The synergetic effect between the metal oxide nanoparticles and the conducting polymers, conducting polymer/metal oxide nanocomposite materials show effective results in the removal of cationic dye (methylene blue) molecules. Furthermore, there is an urgent need to develop low-cost, high-efficiency waste water treatment methods. Among the various procedures used to remove dye molecules from wastewater, such as coagulation, photocatalysis, flocculation, reverse osmosis, and membrane separation, adsorption and photocatalytic degradation are simple and cost-effective. It requires less catalyst and produces very few harmful by-products. Semi conducting photocatalytic materials are gaining popularity due to their UV and visible light absorption capacity, stability, and wide range of applications such as dye degradation, catalysis, and antibacterial activity, among others.

Therefore, the semi conducting material like NiO, ZnO, CuO, TiO_2 and SnO draws a significant attention among the researchers owing to their application as optoelectronics, transducers, ultraviolet light emitters, piezoelectric devices, chemical sensors, cosmetics and photocatalyst etc. [1–9]. Among which ZnO nanoparticles is a well-recognized n-type semiconductor with high electron mobility, large exitonic binding

* Corresponding author.
E-mail address: drbadhunano@gmail.com (M.S.M. Badhusha).

https://doi.org/10.1016/j.inoche.2023.110877
Received 23 March 2023; Received in revised form 25 May 2023; Accepted 26 May 2023
1387-7003/

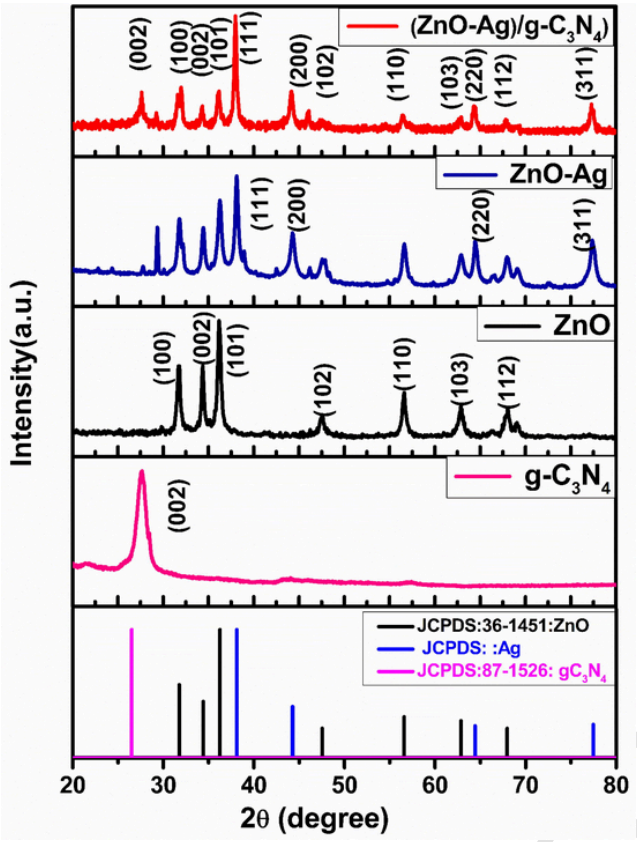

Fig. 1. X-ray diffraction patterns of ZnO, g-C_3N_4, ZnO-Ag NPs, and (ZnO-Ag)/ g-C_3N_4 nanocomposite in comparison with the JCPDS database.

energy, non-toxic, high photo sensitivity and good optical properties for photocatalytic activity [10–20]. Even though the semiconductors couldn't exhibit a highly effective photocatalytic performance due to their fast charging and re combination of electron hole pairs (e^-, h^+). Therefore, to overcome the defect in photocatalytic property of metal oxide we can introduce a dopant or design a nanocomposite structure of metal and nonmetal (act as electron acceptor). By which we can suppress the electron and hole recombination and increase the charge separation for enhanced optical properties. [21–24].

The S-scheme heterojunction has drawn increased interest in the photocatalytic sector due to its strong photo-generated charge carrier redox capacity and spatial separation. The two types of n-type semiconductor photocatalysts that make up the S-scheme heterojunction photocatalyst are the reduction photocatalyst (RP) with a negative CB site and the oxidation photocatalyst (OP) with a positive VB site. The internal electric field (IEF) is the main source of driving force for carrier transfer in a typical S-scheme heterojunction device. Electrons move from the CB of the RP to the VB of the OP under the influence of the IEF that exists at the interface between the two semiconductors. In addition, the IEF can stop electrons from moving continuously from RP to OP.

According to the previous reported data, ZnO, Ag work function values are 5.2 eV and 4.26 eV, respectively. When two materials with distinct work functions are mixed, a Schottky barrier typically forms. As a result, electrons will go from the material with a lower work function to the material with a higher work function. Due to the larger work function of Au and Ag, their Fermi levels (FM) are higher than ZnO's (F_{MO}). this controls the movement of electrons from the Ag to the ZnO Fermi levels until equilibrium is reached and form a new equilibrium Fermi level (F_{Eq}). The surface of the metal was left with holes after the visible light irradiation because the surface phonon resonance (SPR) mechanism was used to quickly inject the electrons in FEq into the conduction band (CB) of ZnO. Now, the electrons pumped into CB react with dissolve oxygen, creating superoxide radical anion (O2• -), which can then react with H_2O to form hydroxyl radicals (OH•) in a subsequent reaction pathway. The MB dye pollutant are broken down by these superoxide radical anion and hydroxyl radicals when exposed to visible light [25].

The previously reported ZnO combination with noble metal like Co, Au, Ag, Cu, Pd shows an optimum band gap for strong visible light absorption, increase in photocatalytic performance by surface plasmon resonance effect and ability to form Schottky junction [26–30]. But the modification of ZnO nanoparticles with Ag nanoparticles has wide variant of applications like non-toxicity, catalytic potential, etc. The silver NPs requires a simple synthesis condition which makes it suitable for making Ag based nanocomposite materials. Due to its surface volume ratio Ag is used in bactericide purpose and catalyst for dye degradation. [31–36].

Since dopant alone cannot provide the anticipated result for photo catalytic performance. Researchers are searching for a new way to make use of conjugating material such as graphene, carbon nano tube, g-C_3N_4 and C_{60} etc. In which the g-C_3N_4 fabricate NPs s shows a high adsorption capacity, porous structure, thermal stability, chemical stability, large surface area and adequate charge carrier capacity. Moreover, it has moderate band gap (2.7ev) which yields the good photocatalytic conversion of water into hydrogen gas under sun light [37–47]. Besides being organic semi conducting material, g-C_3N_4 could be easily prepared through various precursor melamine, urea, and thiourea which are of low cost. Also, it is a structurally stable aromatic polymer which can be easily applied to other material surfaces [48–49].

Although various chemical and physical methods are available for the synthesis of (ZnO-Ag)/g-C_3N_4 nanocomposites. There are no reports related to the green synthesis of (ZnO-Ag)/g-C_3N_4 nanocomposites which could be an ecofriendly, low cost, simplicities, development of more stable and biocompatible nanoparticles. The plant extract contains sugars, terpenoids, phenolic compound, alkaloids, flavonoid, and proteins acting a major role in the reduction of metal ions into NPs [50–53]. In this is the first work, we report the novel synthesis of (ZnO-Ag)/g-C_3N_4 nanocomposites using the leaf extract of *T. Arjuna,* belonging to Combretaceae family. The structure and morphology of the prepared Nanocomposite were studied by using XRD, UV–Vis FT-IR, XPS, PL, TEM and BET analysis. In application part the photodegradation of methylene blue and antibacterial against gram (+) ve bacteria and gram (-) ve bacteria was examined and compared with g-C_3N_4, ZnO, ZnO-Ag NPs and (ZnO-Ag)/g-C_3N_4 nanocomposite.

2. Materials and method

2.1. Materials

T.Arjuna leaves were collected from Tirunelveli district, Tamil Nadu, India. Zinc acetate dihydrate (Zn $(CH_3COO)_2$. 2 H_2O), silver nitrate ($AgNO_3$), urea (CH_4N_2O), ethanol (C_2H_6O) and methylene blue ($C_6H_{18}ClN_3S$) were purchased from Merck. The procured chemicals were of analytical grade and utilized without any treatment.

2.2. Preparation of leaf extract of T.Arjuna

The leaf of T. Arjuna was chopped into small pieces and then washed with distilled water to eliminate any adhering salts or other impurities. The leaf was allowed to dry for seven days at room temperature and grounded into a fine powder. Using a magnetic stirrer, 100 mL of distilled water and a 5 g of dried leaf powders were continuously stirred for 30 min. This extract was then centrifuged twice for 10 min at 4500 rpm. Finally, the supernatant solution was filtered using Whatman filter paper and kept at 4 °C.

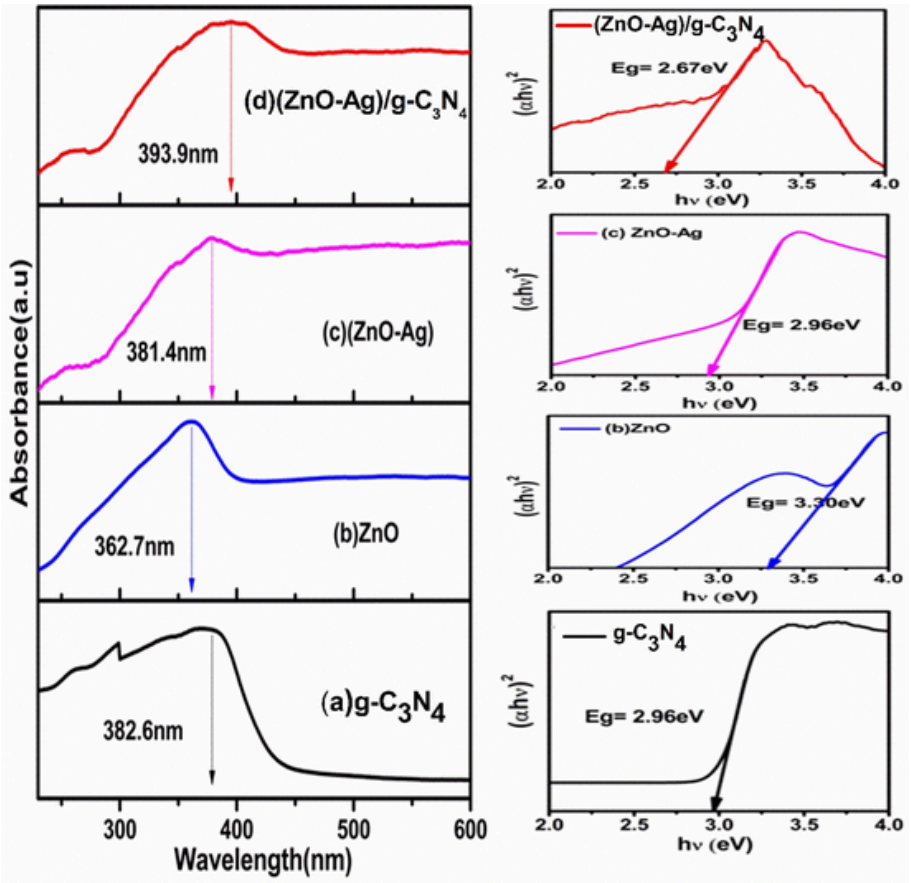

Fig. 2. The absorption range of synthesised ZnO, g-C_3N_4, ZnO-Ag NPs,(ZnO-Ag)/ g C_3N_4 nanocomposite and their determined band gap values.

2.3. Synthesis of g-C_3N_4

The g-C_3N_4 powder was synthesized by pyrolysis of urea. 10 g of urea was placed in an alumina crucible with a lid and heated in a muffle furnace to 550 °C for 3 h at a rate of 5 °C/min. The resulting pale-yellow g-C_3N_4 was collected and ground into powder for further use.

2.4. Synthesis of ZnO NPs using T.Arjuna

Initially, 0.1 M of zinc acetate was mixed with 50 mL of de ionized water and stirred vigorous for half an hour at 70–80 °C. Then the *T.Arjuna* leaf extract was added dropwise to the zinc acetate solution. As a result of the reaction was the formation of the dirty colored precipitate. This mixture was centrifuged at 6000 rpm for 15 min, and the precipitate was repeatedly washed in deionized water and ethanol to remove contaminants. This residual precipitate was dried in an oven at 80 °C. Finally, the as-prepared sample was calcined to 500 °C in a muffle furnace for two hours.

2.5. Synthesis of ZnO-Ag NPs using T.Arjuna

0.1 g of ZnO was dispersed in 50 mL aqueous solution under vigorous stirring for 30 min. silver nitrate solution was prepared by dissolving 0.01 g of silver nitrate dissolved in distilled water, and was then mixed with the aqueous ZnO suspension. And then 10 mL leaves extract of T.Arjuna was added to the above solution under vigorous stirring for 2 h. The resulting ZnO-Ag NPs was separated by filtration, washed with distilled water and ethanol and further dried overnight at 80 °C.

2.6. Synthesis of (ZnO-Ag)/g-C_3N_4 nanocomposite

The (ZnO-Ag)/g-C_3N_4 nanocomposite was prepared by ultrasonic treatment as follows: 0.5 g of g-C_3N_4 and 0.02 g of ZnO-Ag NPs were added into 50 mL of water and then, the suspension was ultrasonicated for 45 min to obtain a homogeneous solution. Afterward, the mixture was centrifuged and washed with water and ethanol, then dried hot air oven at 100 °C for 6 h. Finally, (ZnO-Ag)/g-C_3N_4 nanocomposite were obtained.

2.7. Characterizations

The X-ray diffraction (XRD) patterns were recorded using PAN analytical XPert PRO-powder X-ray diffractometer with a Cu- Kα radiation (λ = 1.541 Å). High Resolution Transmission Electron Microscope 9 JEOL-2100 + was used to analyze the morphology of the Nanocomposite. Using Thermo Nicolet 380 model, Fourier transform infrared (FTIR) spectroscopy was recorded to determine the functional group. X-ray photoelectron spectrometer (VERSAPROBE III) was used to confirm the elemental composition. UV–visible spectroscopy (ELICO S1164) was used to characterize the optical properties of the material.

2.8. Photocatalytic activity measurement

The photocatalytic activity of the synthesized g-C_3N_4, ZnO, ZnO-Ag NPs and (ZnO-Ag)/g- C_3N_4 nanocomposite has been investigated via dye degradation of methylene blue in aqueous solution. Methylene blue was pick out to explore the catalytic activity of g-C_3N_4, ZnO, ZnO-Ag NPs and (ZnO-Ag)/g-C_3N_4 nanocomposite in this catalytic experiment 50 ppm of dye taken and added the 50 mg of catalyst. This solution kept in dark for to attain the adsorption- desorption equilibrium. After

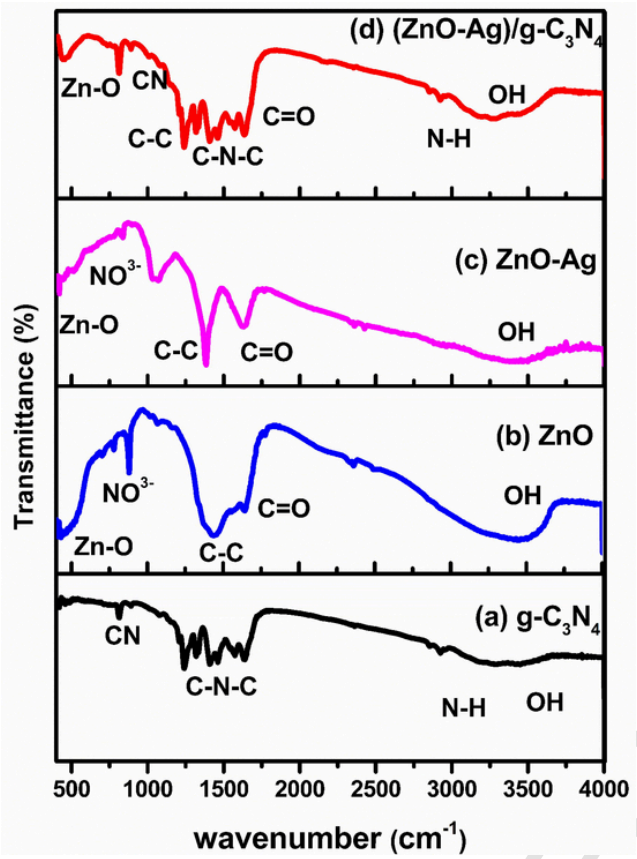

Fig. 3. The presence of functional group in the synthesized ZnO, g-C_3N_4, ZnO-Ag NPs, (ZnO-Ag)/ g-C_3N_4 naocomposite.

30 min the reaction mixture irradiated with UV light and 2 mL of slurry was taken at different intervals (20, 40 and 60 min). This dye solution was analyzed by UV visible spectrometer to recognise the degradation of dye. The % degradation of dye was calculated by using the formula.

% of degradation = C_0-C/$C^{0\times}$ 100 1.

Photocatalysis mechanism: The reduction and oxidation processes define a photocatalyst's role in the existence of light photons. the photocatalytic reaction that occurs after the three steps listed below:

o Electron and hole generation (photo-excitation).

o Electron and hole separation and diffusion into the catalyst surface.

o Reactions of photoreduction and photooxidation on the catalyst surface.

The photocatalytic process is influenced by the following factors:

Temperature of the photocatalytic reaction, Pollutant concentration and amount of catalyst in wastewater, pH of the medium, Light photon intensity, Wavelength of incident light photon, Oxygen content and Presence of ionic compounds.

The Strategies for creating highly effective and stable photocatalysts include:

(1) coupling semiconductors with other semiconductors to meet high solar energy absorption requirements and to generate enough built-in potential for redox reactions.

(2) forming heterostructured junctions with carbon material to efficiently drive the separation and transportation of the electron-hole pairs.

(3) the creation of multicomponent heterojunctions to improve the separation/transport of electron-hole pairs and the use of sunlight. The advancements made in this area suggest that creating heterojunctions is a viable option for improving the photocatalytic efficiency of semiconductors.

2.9. Antibacterial activities

The antibacterial activity of the bio-synthesized g-C_3N_4, ZnO, ZnO-Ag NPs and (ZnO-Ag)/g-C_3N_4 nanocomposite were investigated against the pathogenic bacteria such as gram-positive *Bacillus subtilis* (G +) and Gram-negative pathogens *Protius Mirabilis* (G-) bacteria using disc diffusion method. The pathogenic germs were injected in a nutritional broth and incubated for 12 h at 37 °C. The test pathogenic cultures that had been cultivated overnight were swabbed onto Muller-Hinton agar (MHA) plates. Then, water was used as a negative control while the produced g-C_3N_4, ZnO, ZnO-Ag NPs and (ZnO-Ag)/g-C_3N_4 nanocomposite were added to the disc. The identified inhibitory zone was measured when the plates were incubated overnight at 37 °C.

3. Results and discussion

3.1. Structural property

Fig. 1 The structural confirmation of g-C_3N_4, ZnO, ZnO-Ag NPs and (ZnO-Ag)/g-C_3N_4 Nanocomposite was carried out using X ray diffraction technique, which reveals that the Terminalia Arjuna leaf extract has acted as an excellent reducing and capping agents for material synthesis, as observed from the crystalline nature of the X-ray diffraction pattern. The phase purity of samples in comparison with JCPDS database and the successful incorporation of one compound into another is evident from Fig. 1. The peaks located at (1 0 0), (0 0 2), (1 0 1), (1 0 2), (1 1 0), (1 0 3) and (1 1 2) h k l planes correspond to the phase pure synthesis of hexagonal structured ZnO nanoparticles holding a good record with JCPDS No: 36–1451. The incorporation of Ag nanoparticles into ZnO was confirmed by the diffraction of (1 1 1), (2 0 0), (2 2 0) and (3 1 1) h k l planes indicating the phase pure synthesis of silver metal nanoparticles in accordance with the JCPDS No: 89–3722. The characteristic peak of phase pure g-C_3N_4 was observed at 26.5^0 having a good match with the JCPDS No: 87–1526. Hence the successfully synthesized (ZnO-Ag)/g-C_3N_4 Nanocomposite without any secondary phases was furthered employed in photocatalytic application.

3.2. Optical property

Since the photocatalytic performance of the material depends upon the optical property of the compound. The band gap values of the g-C_3N_4, ZnO, ZnO-Ag NPs and (ZnO-Ag)/g-C_3N_4 Nanocomposite were analyzed using UV–visible spectroscopy. Fig. 2 illustrates the absorption region for g-C_3N_4, ZnO, ZnO-Ag NPs and (ZnO-Ag)/g-C_3N_4 nanocomposite lying around, 382.6 nm, 362.7 nm 381.4 nm, and 393.9 nm respectively, this indicates that the absorption edge of ZnO-Ag NPs is extended to the visible light range, when compared to pure ZnO NPs is due to the integration of ZnO with Ag and the surface plasmon resonance effect of silver[54]. Using Tauc's relation given in equation.2 the band gap values were determined.

$$(\propto h\nu)^n = K\left(h\nu - E_g\right) \cdots\cdots\cdots\cdots\cdots\cdots (2)$$

Here, α represents absorption coefficient, Eg denotes optical band gap, K is a proportionality constant, h refers to plank's constant, and ν denotes the frequency, n = 2 indirect bandgap. The determined band gap values are 2.96 eV, 3.30 eV, 2.96 eV, 2.67 eV for g-C_3N_4, ZnO, ZnO-Ag NPs and (ZnO-Ag)/g-C_3N_4 Nanocomposite respectively. The decrease in bandgap energy owing to its absorption towards the visible region. This shift might be indorsed to sp-d spin interchange involving the localized d electrons of the dopant Ag and band electrons of the host ZnO and increase in the oxygen vacancies in the crystal structures. Also, might be due to the synergistic effect and heterojunction formed between ZnO-Ag and g-C_3N_4. Furthermore, this decreases in bandgap value, the material can induce more photo carriers in the presence of

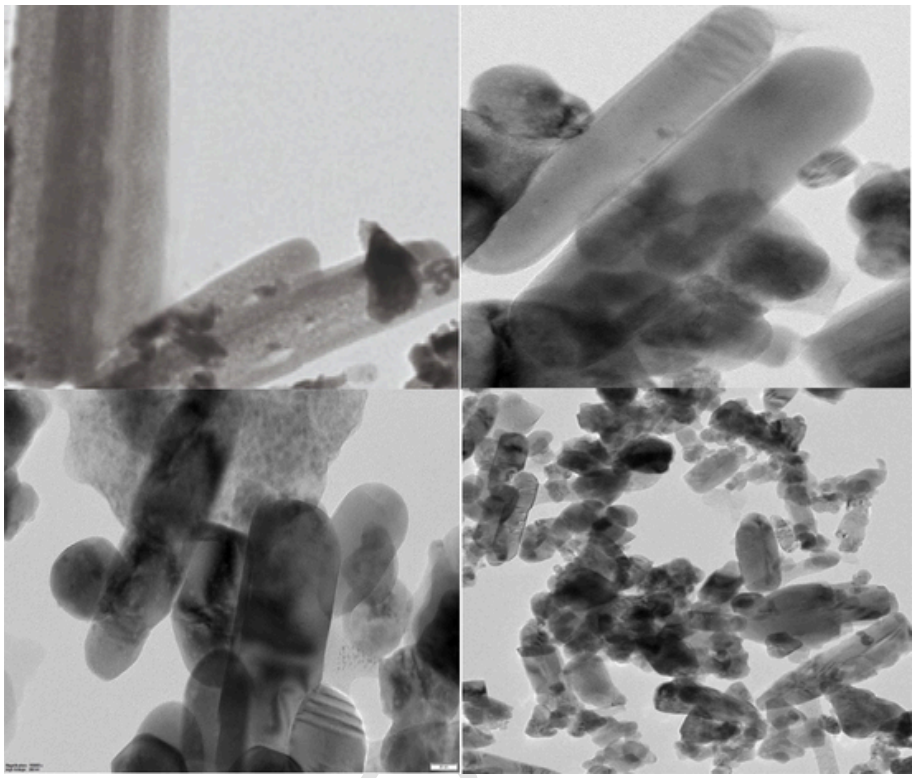

Fig. 4. Morphology of synthesized ZnO, g-C_3N_4, ZnO-Ag NPs, and (ZnO-Ag)/ g-C_3N_4 nanocomposite.

sunlight as a medium. The synergistic interaction between Ag NPs, exfoliated g-C_3N_4, and ZnO play a significant role in light harvesting and energy band matching which is a potential optical property for practical applications. This difference in band gap value of ZnO with 3.30 eV and 2.67 eV for (ZnO-Ag)/g-C_3N_4 nanocomposite illustrates the successful interaction of ZnO, Ag, and g-C_3N_4 nanomaterials.

3.3. FTIR Analysis:

The presence of hydrate groups, metal bonding and other functional groups due to organic compounds were analyzed using Fourier Transform Infra-red spectroscopy (FTIR) shown in Fig. 3. Three prominent bands were observed in the range of 3000–3600, 1200–1650 and 810 cm^{-1}. The broad peak around 3000–3600 cm^{-1} corresponds to the stretching vibration of N–H in uncondensed amine groups, –OH groups, and the stretching mode of CN heterocycles. The repeating stretching vibration produced by heptazine was observed at 1632, 1478, and 1405 cm^{-1}. The peaks at 1320 and 1235 cm^{-1} attributes to the stretching vibration of C—N(—C)—C. The primary building block of g-C_3N_4 such as tri-s-triazine ring's out-of-plane bending was recognized from the peak at 810 cm^{-1}. The band observed at 440 cm^{-1} was attributed to the stretching vibration of metal bonding, confirming the presence of Zn-O bond. The characteristic peak at 1631 cm^{-1} can be attributed to the C = O groups. The absorption band at 1410 $cm^{-1}$and could be attributed C–C vibration respectively. The main component present in the leaf extract of *T. arjuna* such as leucoanthocyanidins, arjunetin and hydrolyzable tannins are responsible for the reduction of reduction of precursor into nanoparticles. These results indicate that phytochemicals present in the plant extract is responsible for the successful synthesis of (ZnO-Ag)/g-C_3N_4 Nanocomposite.

3.4. TEM analysis

The morphology of the synthesized g-C_3N_4, ZnO, ZnO-Ag NPs and (ZnO-Ag)/g-C_3N_4 Nanocomposite was analyzed using Transmission electron microscope (TEM). Fig. 4(a) shows the nano formation of pristine g-C_3N_4. The observed rod like structures shown in Fig. 4(b) illustrates the formation of rod shaped ZnO nanoparticles. The successful incorporation of Ag NPs in ZnO nanoparticles can be clearly seen through Fig. 4(c), the dark spot in ZnO rods corresponds to Ag NPs. Finally, Fig. 4 (d). displays the TEM image of synthesized ZnO-Ag)/g-C_3N_4 nanocomposite.

3.5. XPS spectra

X-ray photoelectron spectroscopy was used to evaluate the surface chemical composition and oxidation state of the synthesized (ZnO-Ag)/g-C_3N_4 nanocomposite. Fig. 5 (a) displays the survey spectrum of (ZnO-Ag)/g-C_3N_4 nanocomposite indicating the presence of C, N, Zn, Ag and O elements only with a weight percentage of 47.5%, 43.8%, 1.2%, 1.3% and 6.1% respectively. This confirms the phase purity of the sample by the absence of secondary phases. The high resolution XPS spectra reveals out the presence of Zn 2p core level located at 1021.0 eV and 1044.2 eV, which corresponds to Zn $2p_{2/3}$ and Zn $2p_{1/2}$ respectively. The separation between both the peaks is equals to 23.0 eV, this holds a good agreement with the previous literatures indicating the presence of Zn^{2+} state in ZnO nanoparticles shown in Fig. 5 (b). The peak centered at 530.4 eV is ascribed to O 1 s spectrum displayed in Fig. 5 (c). The peak centered at 530.4 eV is ascribed to O 1 s spectrum attributed to oxygen-deficient regions of the ZnO and lattice oxygen displayed in Fig. 5 (c). The deconvoluted peaks of C1s at 285.06 eV, and 288.1 eV attributes to sp^2-hybridization of C-N and C-N = C in g-C_3N_4 respectively. The peak at 287.07 eV is assigned to C-N-C carbon groups shown in Fig. 5 (d). The predominant peak representing the presence of metallic silver at 366.9 eV and 372.9 eV corresponds to Ag $3d_{3/2}$ and Ag $3d_{5/2}$ respectively displayed in Fig. 5 (f). Thes two peaks has a spin energy separation of 6.0 eV confirming the zero-valent state of metallic Ag. The spectrum of N1s shown in Fig. 5 (e) indicates the peak at 398.01 eV referring to nitrogen in triazine ring and heterocyclic rings. From these results, we can conclude that the

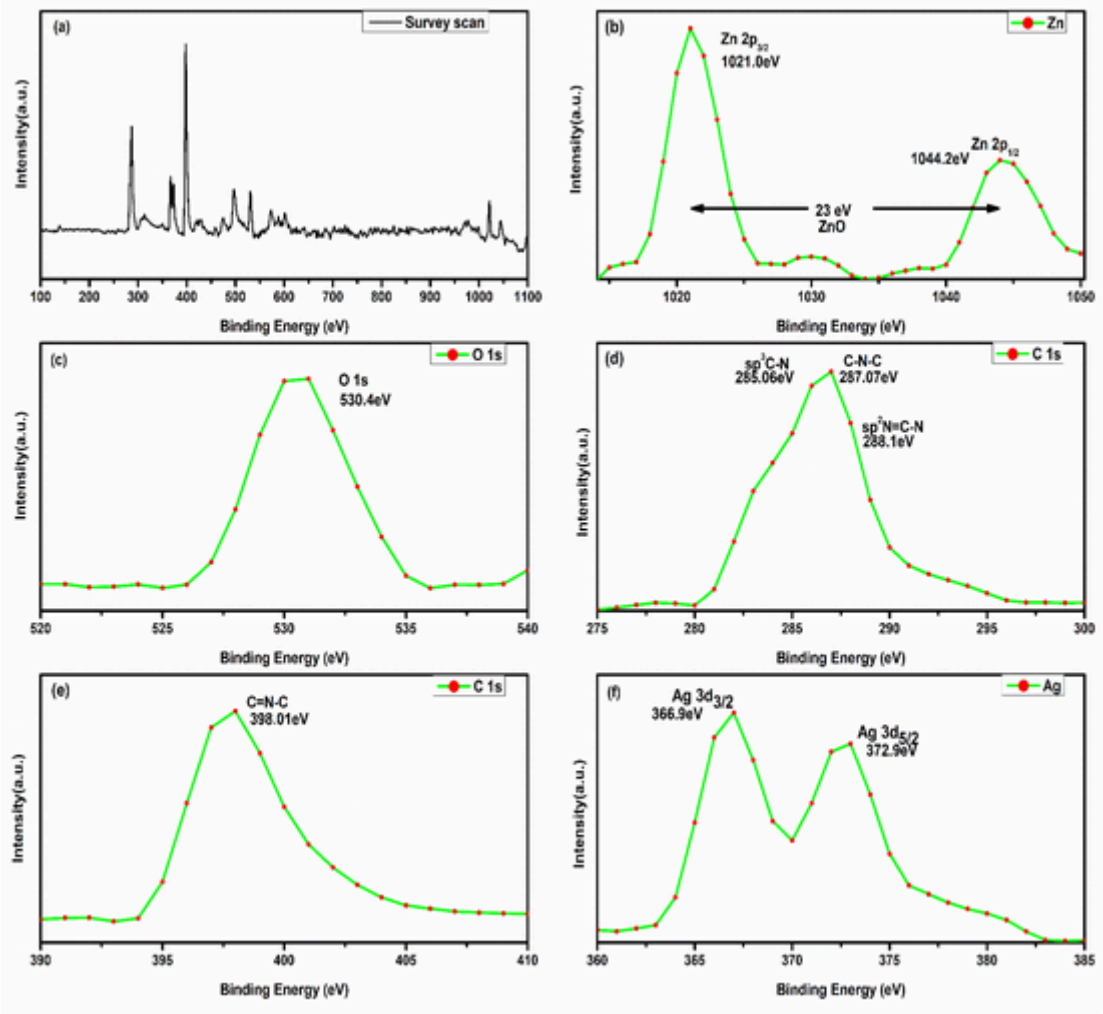

Fig. 5. XPS analysis of the synthesized ZnO, g-C_3N_4, ZnO-Ag NPs, (ZnO-Ag)/ g-C_3N_4 nanocomposite.

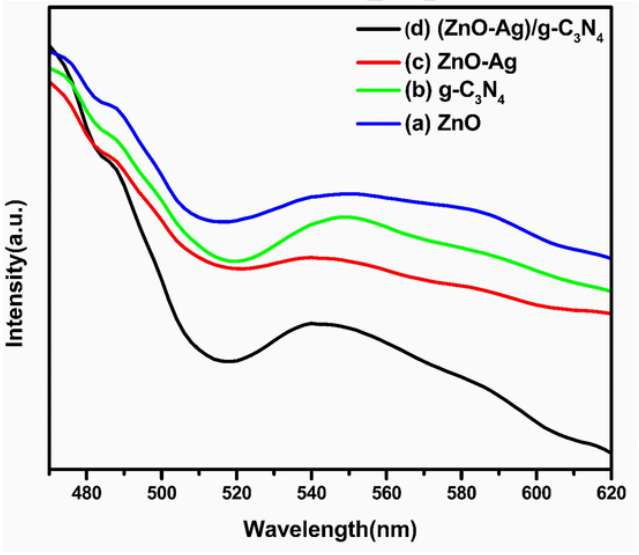

Fig. 6. PL spectra of the pristine ZnO, g-C_3N_4, ZnO-Ag, and (ZnO-Ag)/g-C_3N_4 nanocomposite.

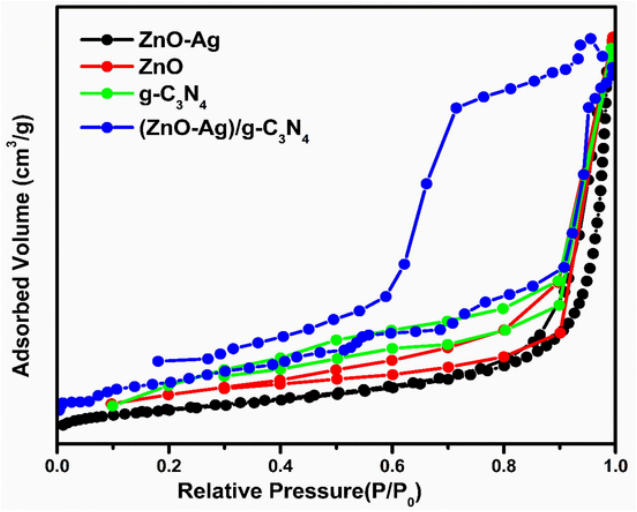

Fig. 7. BET analysis of the pristine ZnO, g-C_3N_4, ZnO-Ag, and (ZnO-Ag)/g-C_3N_4 nanocomposite.

Table 1
The surface area, pore-volume, and average pore width of the synthesized g-C3N4, ZnO, ZnO-Ag NPs, and (ZnO-Ag)/g-C_3N_4 nanocomposite.

Photocatalyst	Surface area (m^2g^{-1})	Pore volume (cm^3g^{-1})	Average pore width (Å)
ZnO	17.37	0.043	145.62
g-C_3N_4	39.04	0.091	123.65
ZnO-Ag	46.62	0.23	96.79
(ZnO-Ag)/g-C_3N_4	68.70	0.275	80.54

XRD results and XPS results goes in hand to hand explaining the successful formation and interaction in (ZnO-Ag)/g-C_3N_4 nanocomposite to be used effectively in photocatalytic activity.

3.6. Photoluminescence spectroscopy

Fig. 6 shows the PL spectrum of synthesized ZnO, g-C_3N_4, ZnO-Ag, and (ZnO-Ag)/g-C_3N_4 nanocomposite recorded at room temperature. As the photoluminescence (PL) spectroscopy is used to identify the level of recombination induced by the photogenerated e-h pairs. The peak intensity of PL spectra indicates the level of recombination of e-h pairs. The ZnO NPs and g-C_3N_4 shows the highest emission peak intensity among all the samples, demonstrating the maximum recombination rate of the e–h pairs. The emission peak intensity of ZnO-Ag was lower than ZnO and g-C_3N_4, signifying that the Ag adding into ZnO prolonged the lifetime of the photo-promoted e–h pairs and partially suppressed the e-h pairs. But the emission spectrum of (ZnO-Ag)/g-C_3N_4 nanocomposite has a lower intensity than other samples, this clearly states that the e-h pairs were significantly suppressed in the (ZnO-Ag)/g-C_3N_4 nanocomposite due to the synergistic effect among pure ZnO, Ag NPs, and g-C_3N_4. Due to this suppressed recombination behavior in (ZnO-Ag)/g-C_3N_4 nanocomposite could be able to exhibit a better photocatalytic activity among the synthesized samples. The overall lifetime of photo promoted electrons of prepared samples was in the following order, (ZnO-Ag)/g-C_3N_4 > ZnO-Ag > g-C_3N_4 > ZnO.

3.7. BET analysis

The synthesized sample were further characterized by Brunauer-Emmett-Teller (BET) technique to determine the surface area, pore size and pore volume. Fig. 7 depicts the N_2 adsorption/desorption pattern for the ZnO, g-C_3N_4, ZnO-Ag, and (ZnO-Ag)/g-C_3N_4 nanocomposite sample. The development of a hysteresis loop at a higher partial pressure indicates that voids exist in the nanocomposite sample according to IUPAC classification. The greater surface area of the (ZnO-Ag)/g-C_3N_4 nanocomposite compared with other sample can promote the growth and number of surface-active sites. Larger the surface areas will create more active sites this helps the photocatalyst to adsorb more pollutants onto the surface. Consequently, the maximum amount of the pollutants might be adsorbed and degraded by the (ZnO-Ag)/g-C_3N_4 compared to other samples is tabulated in Table 1.

3.8. Photocatalytic activity

The degradation rate of MB under UV light irradiation was evaluated to investigate the photocatalytic activity of g-C_3N_4, ZnO, ZnO-Ag NPs, and (ZnO-Ag)/g-C_3N_4 nanocomposite. To fulfil this, 50 mg photocatalyst was dispersed in 80 mL of MB aqueous solution with an initial

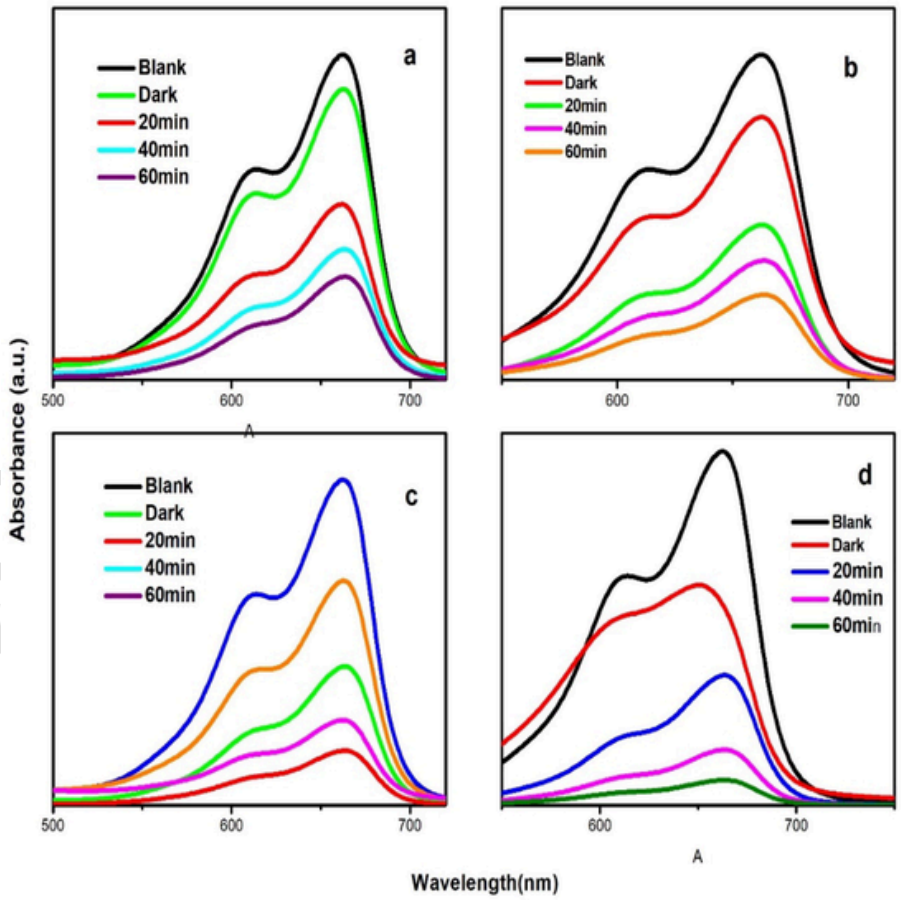

Fig. 8. Comparison of the MB photodegradation in different specimen a)ZnO b) g-C_3N_4 c)ZnO-Ag NPs d) (ZnO-Ag)/g-C_3N_4 nanocomposite.

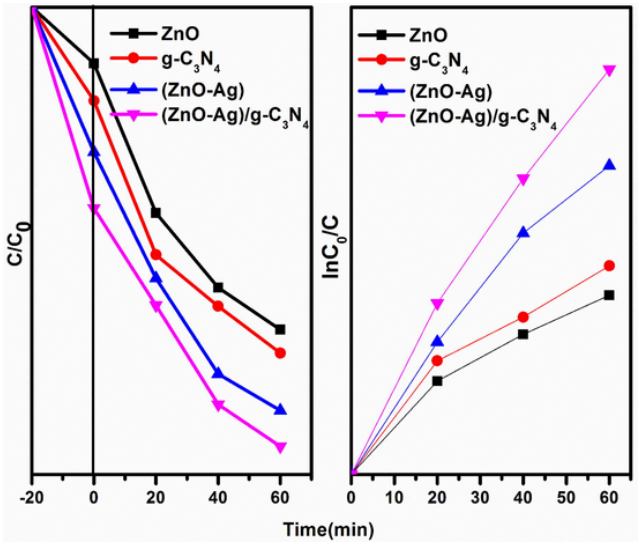

Fig. 9. (a) Photodegradation efficiency (b) Kinetic plot of MB degradation on ZnO, g-C_3N_4, ZnO-Ag NPs, (ZnO-Ag)/g-C_3N_4 nanocomposite.

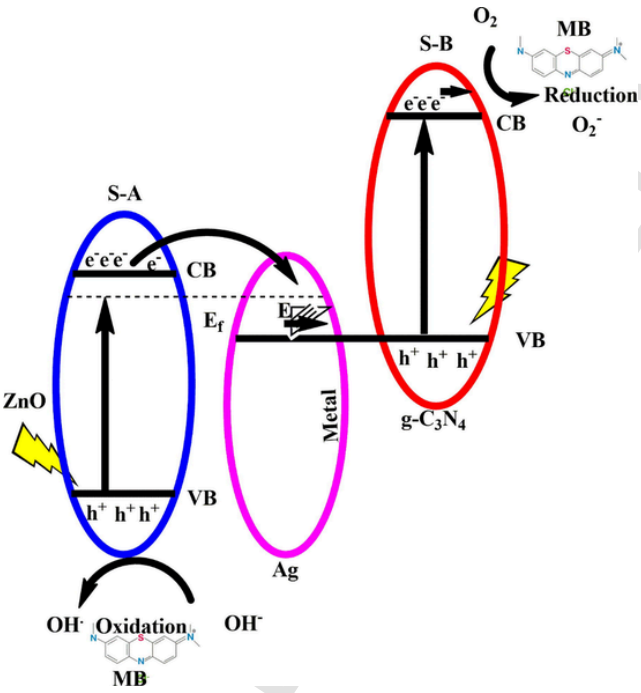

Scheme 1. Schematic illustration of photocatalytic degradation of MB dye by (ZnO-Ag)/g- C_3N_4 nanocomposite.

Table 2
The calculated rate constants (k), correlation coefficients (R^2), for maximal dye degradation in the presence of g-C3N4, ZnO, ZnO-Ag NPs, and (ZnO-Ag)/g-C_3N_4 nanocomposite.

Sample	R^2	K (min^{-1})
ZnO	0.9811	0.0165
g-C_3N_4	0.9828	0.0208
ZnO-Ag	0.9919	0.0277
(ZnO-Ag)/g-C_3N_4 NCs	0.9961	0.0351

concentration of 50 mg/L under magnetic stirring; the suspension was then stirred in the dark for 30 mins to establish an adsorption–desorption equilibrium between the MB and the photocatalyst. The suspension was then subjected to 1 h of UV irradiation with a 654 nm cut-off filter. At each time interval, a 2 mL suspension of the reaction solution was removed and centrifuged to obtain a clear solution. The absorbance of MB was measured at the wavelength of maximum absorption. Finally, the photocatalytic degradation efficiency was calculated using time profiles of C_t /C_0, where C_0 is the initial concentration of MB and C_t is the concentration after t minutes of irradiation.

The blank test confirms that MB degradation is statistically insignificant in the absence of catalysts. The maximum absorption intensity of MB dye gradually decreased, indicating that cationic dyes selectively interact with nanocomposites and are removed from solution. The results clearly show that the degradation efficiency of g- C_3N_4 and ZnO NPs was 75% and 68%, respectively. Furthermore, after doping the ZnO nanoparticles with Ag, the catalytic activity gradually increased. ZnO-Ag degradation efficiency was 80%. Furthermore, degraded MB efficiently of prepared samples in the order (ZnO-Ag)/g-C_3N_4 > ZnO-Ag > g- C_3N_4 > ZnO. At the end of the experiment, 94% of the MB was removed in 60 min, and the dye colour was changed from deep blue to colorless solution which ensures the complete removal of dye shown in Fig. 8 (a, b, c and d) for g-C_3N_4, ZnO, ZnO-Ag NPs, and (ZnO-Ag)/g-C_3N_4 nanocomposite respectively.

The kinetics of MB degradation by photocatalysts were also studied, with the pseudo-first-order reaction being used to fit the degradation process: ln C_0/C = kt, where k (min^{-1}) represents the first order rate constant, and C_0 and C corresponds to time t concentration of MB. Fig. 9 (a) depicts the kinetics of MB degradation with various samples. Fig. 9 (b) clearly shows that the degradation of MB follows a pseudo first-order kinetics equation. The observed results clearly demonstrate that the prepared photocatalyst followed pseudo-first-order kinetics. Table 2 shows the calculated rate constants (k), correlation coefficients (R^2), for maximal dye degradation in the presence of g-C_3N_4, ZnO, ZnO-Ag NPs, and (ZnO-Ag)/g-C_3N_4 nanocomposite are given Table 2. The estimated k values for g-C_3N_4, ZnO, ZnO-Ag NPs, and (ZnO-Ag)/g-C_3N_4 nanocomposite were 0.0208, 0.0165, 0.0277, and 0.0351 min-1. The incorporation of prepared samples significantly increases the highest degradation, the k rate of (ZnO-Ag)/g-C_3N_4 composites observed is 0.0351 min^{-1}, which is approximately 2.1 times that of 0.0165 min^{-1} for pure ZnO.

Scheme 1 depicts First off, since semiconductors A (S-A) and B (S-B) both have different photoabsorption ranges and can be activated by UV/visible light, combining their photoabsorption can increase the range of UV/visible-light photoresponse. Second, the photocatalytic reaction is started by UV/visible light photons that have an energy that is equal to or higher than the band gap in both S-A and S-B. This causes the formation of photogenerated holes in their VB and electrons in their CB. In the other hand, the Fermi level of S-A is higher compared to the loaded metal, which is similar to the previous reports of electron transfer from a semiconductor (such as TiO_2) to metal (such as Ag, Au), so the electrons in the CB of S-A easily flow into metal (electron transfer I: S-A - metal) through the Schottky barrier. Compared to the electron-hole recombination between the VB and the CB of S-A, this electron transfer I process is quicker. As a result, the metal component can store a large number of the electrons in the S-A CB, more holes with a strong oxidizing power, escapes from the S-A's VB recombination behavior and are able to freely oxidize the OH or contaminants. A faster process than the electron-hole recombination between the VB and CB of S-B occurs when holes in the VB of S-B easily flow into metal because its energy level is higher than that of S-B (electron transfer II: metal - S-B, see scheme. 1). In the CB of the S-B, more electrons with a strong reduction power can elude pair recombination and become available to decrease some absorbed substances (such O^2, H+, etc.). Therefore, UV/visible light stimulation of both S-A and S-B can result in simultaneous electron transfer I and II (that is, vectorial electron transfer of S-A - metal - S-B in Scheme.1). Metal in multicomponent heterojunction systems functions as a storage and/or recombination center for electrons in the CB of S-A and holes in the VB of S-B in these

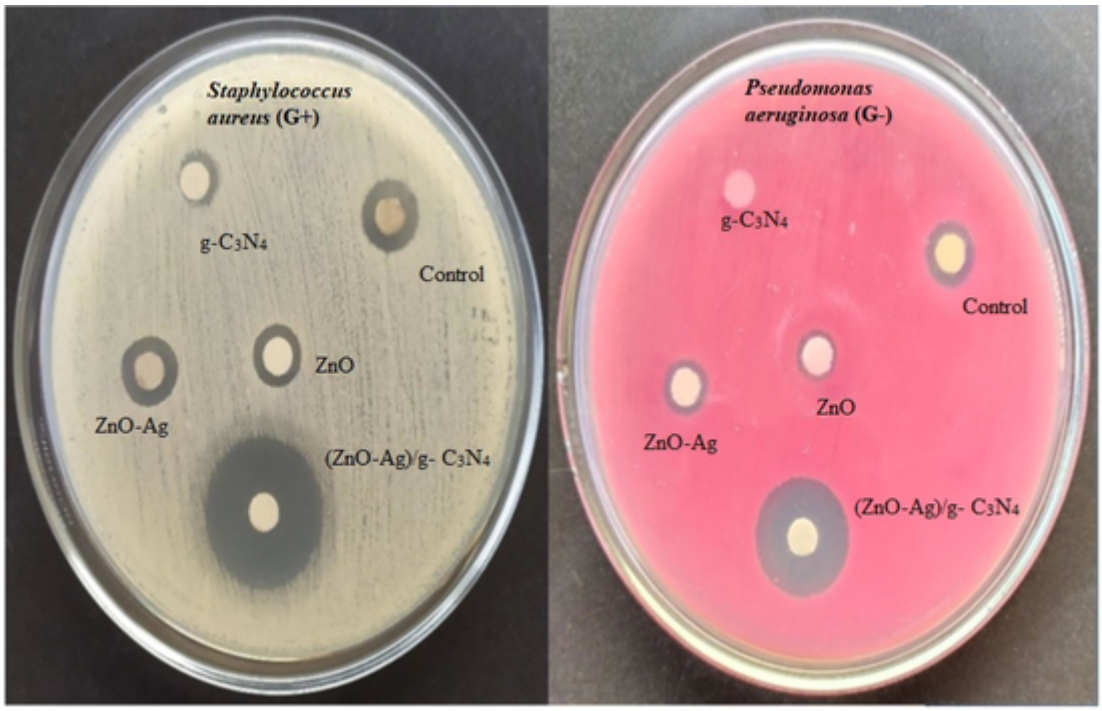

Fig. 10. Photograph of antimicrobial activity of g- C_3N_4, ZnO and ZnO-Ag NPs and (ZnO-Ag)/g- C_3N_4 nanocomposite.

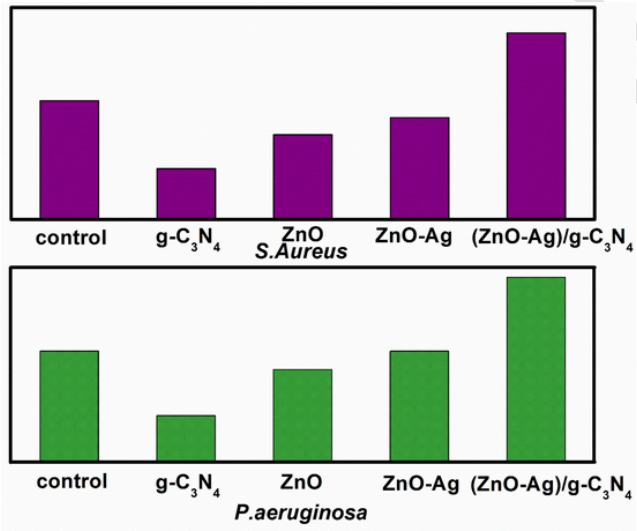

Fig. 11. Bar representation of improved antibacterial activity of synthesized (ZnO-Ag)/ g-C_3N_4 nanocomposite compared to pristine ZnO, g-C_3N_4, ZnO-Ag NPs.

Table 3
Antimicrobial activity of synthesized g-C3N4, ZnO, ZnO-Ag NPs, and (ZnO-Ag)/g-C_3N_4 nanocomposite.

Type of pathogenic	P	Zone inhibition in mm			
		gC_3N_4	ZnO	ZnO-Ag	(ZnO-Ag)/g-C_3N_4 NCs
Staphylococcus aureus (G +)	14	6	10	13	23
Pseudomonas aeruginosa (G-)	12	5	10	12	20

vectorial electron-transfer processes, which helps to improve interfacial charge transfer and realize the complete separation of holes in the VB of S-A and electrons in the CB of S-B. Thus, the holes in VB of S-A has a stronger oxidation power and the electrons in the CB of S-B has a stronger reduction power resulting in the significant enhancement of photocatalytic activity when compared to the previous reported single semiconductor or semiconductor heterojunctions [55–57].

3.9. Antibacterial activities

The antibacterial activity of synthesized g-C_3N_4, ZnO, ZnO-Ag NPs, and (ZnO-Ag)/g-C_3N_4 nanocomposite against Gram-positive pathogens Bacillus subtilis (G +) and Gram-negative pathogens Protius Mirabilis (G-) bacteria was tested using the standard disc diffusion method shown in Fig. 10. An equal amount of each photocatalyst was placed in an agar plate with bacteria and incubated for 24 h. The zone of inhibition against the two bacterial strains was measured for all synthesized samples, as shown in Fig. 11. The results showed that no zone of inhibition was observed in the case of the control disc, implying that distilled water, as a solvent, has no effect on the tested pathogens. g-C_3N_4 had no discernible clear area around the particles, indicating that it has low antibacterial activity. ZnO and ZnO-Ag NPs, on the other hand, showed a small clear area around the particles due to their antibacterial activity. (ZnO-Ag)/g-C_3N_4 nanocomposite demonstrated the highest antibacterial activity against all bacterial strains tested. The larger diameter inhibition zone in (ZnO-Ag)/g-C_3N_4 nanocomposite clearly indicates the effect of Ag NPs and the stability of Ag NPs on the antibacterial properties of the nanocomposite. Table 3 shows the results of an increase in the generation of reactive oxygen species caused by a decrease in the bandgap of ZnO. The antibacterial action of the synthesized samples is listed. Furthermore, Table 3 shows that Gram negative bacteria have a larger inhibition zone than Gram positive bacteria for the two types of materials, which is likely due to Gram positive bacteria's thick cell walls.

The potential antibacterial activity of nanocomposites is depicted in Fig. 10. However, the true mechanism of such antibacterial activity is still unknown. When exposed to light, the synthesized samples produce

e-h pairs in the intended mechanism. The ROS was produced by the interaction of photogenerated e-h pairs with O_2 and H_2O. ROS also migrate to the bacterial surface and cause cell wall rupture. Increased ROS generation due to ZnO's reduced bandgap and g-C_3N_4 large surface area for surface interaction of nanocomposite with the bacterial membrane could explain the enhanced antibacterial activity of (ZnO-Ag)/g-C_3N_4 nanocomposite. Furthermore, Ag NPs can interact with the components of the bacterial cell membrane, causing structural changes, membrane breakdown, and, ultimately, cell death. Similar to this, Ag NPs condensed deoxyribonucleic acid (DNA) molecules, causing DNA to lose its ability to reproduce and cellular proteins to become inactive, both of which cause harm or even death to microorganisms. The combined effect of Ag, ZnO, and g-C_3N_4 results in (ZnO-Ag)/g-C_3N_4 nanocomposite with improved antibacterial activity.

4. Conclusions

T. Arjuna leaves extract was used for the first time, in a novel approach, for green synthesis of (ZnO-Ag)/ g-C_3N_4 nanocomposite. The presence of phenolics compounds in *T. Arjuna* leaves extract has served as both reducing and capping agents in the synthesis of well crystalline and phase pure (ZnO-Ag)/ g-C_3N_4 nanocomposite confirmed using XRD XPS, and TEM. In focus to the optical property the reduction in band gap value and an extended visible region absorption makes the material suitable for photocatalytic application examined using UV–Vis spectroscopy. FTIR reveals out the presence of function group employed in the material formation and the metal bonding in ZnO. The XPS analysis proved that Zn, C, N, O and Ag existed with own identity in (ZnO-Ag)/ g-C_3N_4 nanocomposite without any new elements. The antibacterial performance of the synthesised nanocomposite was assessed using the disc diffusion assay against Staphylococcus aureus and P. aeruginosa. Results showed that when compared to pristine g-C_3N_4, ZnO, and ZnO-Ag NPs the (ZnO-Ag)/ g-C_3N_4 nanocomposite shows an excellent photocatalytic degradation of MB and considerable antibacterial activity against Gram-positive and Gram-negative bacteria.

Availability of data and materials

The raw/processed data required to reproduce these findings cannot be shared at this time as the data also forms part of an ongoing study.

CRediT authorship contribution statement

M. MuthuKathija : Data curation, Investigation, Methodology, Visualization, Writing - original draft.

Declaration of Competing Interest

The authors declare that they have no known competing financial interests or personal relationships that could have appeared to influence the work reported in this paper.

Data availability

The data that has been used is confidential.

References

[1] Zhang, Zijie, et al. "Synthesis and Properties of Ag/ZnO/ g-C_3N_4 Ternary Micro/ Nano Composites by Microwave-assisted Method." *Materials Research Express*, vol. 5, no. 1, IOP Publishing, Jan. 2018, p. 015021. *Crossref*, https://doi.org/10.1088/2053-1591/aaa1dc.

[2] S.P. Adhikari, H.R. Pant, J.H. Kim, H.J. Kim, C.H. Park, C.S. Kim, One pot synthesis and characterization of Ag-ZnO/g-C3N4 photocatalyst with improved photoactivity and antibacterial properties, Colloids Surf. A Physicochem. Eng. Asp 482 (2015) 477–484.

[3] Ngullie, Renathung C., et al. "Synthesis and Characterization of Efficient ZnO/ g-C_3N_4 Nanocomposites Photocatalyst for Photocatalytic Degradation of Methylene Blue." *Coatings*, vol. 10, no. 5, MDPI AG, May 2020, p. 500. *Crossref*, https://doi.org/10.3390/coatings10050500.

[4] Shen, Dong, et al. "Synthesized Z-scheme Photocatalyst ZnO/ g-C_3N_4 for Enhanced Photocatalytic Reduction of CO2." *New Journal of Chemistry*, vol. 44, no. 38, Royal Society of Chemistry (RSC), 2020, pp. 16390–99. *Crossref*, https://doi.org/10.1039/d0nj02270e.

[5] B. Li, Y.u. Wang, Y. Zeng, R. Wang, Synthesis of CuO micro-sphere combined with g-C_3N_4 using Cu2O as precursor for enhanced photocatalytic hydrogen evolution, Mater. Lett. 178 (2016) 308–311.

[6] L.i. Li, S.-Q. Sun, Y.-X. Wang, C.-Y. Wang, Facile synthesis of ZnO/g-C3N4 composites with honeycomb-like structure by H2 bubble templates and their enhanced visible light photocatalytic performance, J. Photochem. Photobiol. A Chem. 355 (2018) 16–24.

[7] Ali Bahadur, Shahid Iqbal Hashem O. Alsaab, Nasser S. Awwad and Hala A. Ibrahium Designing a novel visible-light-driven heterostructure Ni–ZnO/S-g-C_3N_4 photocatalyst for coloured pollutant degradation *RSC Adv.*, 2021,11, 36518-36527 Crossref, https://doi.org/10.1039/D0RA09390D.

[8] Ali Bahadur,a Shahid Iqbal, Mohsin Javed, Syeda Saba Hassan, Sohail Nadeem, Ali Akbar, Rami M. Alzhrani, Murefah Mana Al-Anazy, Eslam B. Elkaeed, Nasser S. Awwad, Hala A. Ibrahiumij and Ayesha Mohyuddin, Construction of a binary S-scheme S-g-C_3N_4/Co-ZF heterojunction with enhanced spatial charge separation for sunlight-driven photocatalytic performance RSC Adv., 2022, 12, 23263 https://doi.org/10.1039/D1RA08525E.

[9] M. Sabri, A. Habibi-Yangjeh, S. Rahim Pouran, C. Wang, Titania-activated persulfate for environmental remediation: the-state-of-the-art, Catal. Rev. 65 (1) (2023) 118–173.

[10] Y. Liang, N.a. Guo, L. Li, R. Li, G. Ji, S. Gan, Facile synthesis of Ag/ZnO micro-flowers and their improved ultraviolet and visible light photocatalytic activity, New J. Chem. 40 (2) (2016) 1587–1594.

[11] Park, Tae Joon, et al. "Ultra-thin Coating of g-C_3N_4 on an Aligned ZnO Nanorod Film for Rapid Charge Separation and Improved Photodegradation Performance." *RSC Advances*, vol. 6, no. 92, Royal Society of Chemistry (RSC), 2016, pp. 89944–52. *Crossref*, https://doi.org/10.1039/c6ra16300a.

[12] W. Liu, M. Wang, C. Xu, S. Chen, Facile synthesis of g-C_3N_4/ZnO composite with enhanced visible light photooxidation and photoreduction properties, Chem. Eng. J. 209 (2012) 386–393.

[13] M. Sundrarajan, S. Ambika, K. Bharathi, Plant-extract mediated synthesis of ZnO nanoparticles using Pongamia pinnata and their activity against pathogenic bacteria, Adv. Powder Technol. 26 (5) (2015) 1294–1299.

[14] S. Aiswarya Devi, M. Harshiny, S. Udaykumar, P. Gopinath, M. Matheswaran, Strategy of metal iron doping and green-mediated ZnO nanoparticles: dissolubility, antibacterial and cytotoxic traits, Toxicol. Res. 6 (6) (2017) 854–865.

[15] J. Xie, Q. Wu, One-pot synthesis of ZnO/Ag nanospheres with enhanced photocatalytic activity, Mater. Lett. 64 (3) (2010) 389–392.

[16] Q.I. Rahman, M. Ahmad, S.K. Misra, M. Lohani, Effective photocatalytic degradation of rhodamine B dye by ZnO nanoparticles, Mater. Lett. 91 (2013) 170–174.

[17] M.H. Koupaei, B. Shareghi, A.A. Saboury, F. Davar, A. Semnani, M. Evini, Green synthesis of zinc oxide nanoparticles and their effect on the stability and activity of proteinase K **RSC**, Adv. 6 (48) (2016) 42313–42323.

[18] N. Bala, S. Saha, M. Chakraborty, M. Maiti, S. Das, R. Basu, P. Nandy, Green synthesis of zinc oxide nanoparticles using Hibiscus subdariffa leaf extract: effect of temperature on synthesis, anti-bacterial activity and anti-diabetic activity, RSC Adv. 5 (7) (2015) 4993–5003.

[19] J.-K. Yan, Y.-Y. Wang, L. Zhu, J.-Y. Wu, Green synthesis and characterization of zinc oxide nanoparticles using carboxylic curdlan and their interaction with bovine serum albumin, RSC Adv. 6 (81) (2016) 77752–77759.

[20] M. Sher, S. Shahid, M. Javed, Synthesis of a novel ternary (g-C_3N_4 nanosheets loaded with Mo doped ZnOnanoparticles) nanocomposite for superior photocatalytic and antibacterial applications, J. Photochem. Photobiol. B Biol. 219 (2021) 112202.

[21] Nurfina Yudasari, Rahma Anugrahwidya, Dahlang Tahir, Maria M. Suliyanti, Yuliati Herbani, Cuk Imawan, Munawar Khalil, Dede Djuhana, J. Alloys. Compd. 886 (2021) 16129.1.

[22] S.J. Lee, T. Begildayeva, H.J. Jung, R. Koutavarapu, Y. Yu, M. Choi, M.Y. Choi, Plasmonic ZnO/Au/g-C3N4 nanocomposites as solar light active photocatalysts for degradation of organic contaminants in wastewater, Chemosphere 263 (2021) 128262.

[23] Javed, Mohsin, et al. "Highly Efficient Visible Light Active Cu–ZnO/S- g-C_3N_4 Nanocomposites for Efficient Photocatalytic Degradation of Organic Pollutants." *RSC Advances*, vol. 11, no. 59, Royal Society of Chemistry (RSC), 2021, pp. 37254–67. *Crossref*, https://doi.org/10.1039/d1ra07203j.

[24] H. Liu, L. Zhong, S. Govindaraju, K. Yun, ZnO rod decorated with Ag nanoparticles for enhanced photocatalytic degradation of methylene blue, J. Phys. Chem. Solid 129 (2019) 46–53.

[25] Q. Xu, L. Zhang, B. Cheng, J. Fan, J. Yu, S-Scheme Heterojunction Photocatalyst, S-Scheme Heterojunction Photocatalyst 6 (7) (2020) 1543–1559.

[26] M.A. Qamar, S. Shahid, M. Javed, S. Iqbal, M. Sher, M.B. Akbar, Highly efficient g-C_3N_4/Cr-ZnO nanocomposites with superior photocatalytic and antibacterial activity, J. Photochem. Photobiol. A Chem. 401 (2020) 112776.

[27] V. Vaiano, G. Iervolino, L. Rizzo, Cu-doped ZnO as efficient photocatalyst for the oxidation of arsenite to arsenate under visible light, Appl. Catal. B 238 (2018) 471–479.

[28] Pan, Hui, et al. "Effects of H-, N-, and (H, N)-Doping on the Photocatalytic Activity of TiO_2." *The Journal of Physical Chemistry C*, vol. 115, no. 24, American Chemical Society (ACS), May 2011, pp. 12224–31. *Crossref*, https://doi.org/10.1021/jp202385q.

[29] K.M. Lee, C.W. Lai, K.S. Ngai, J.C. Juan, Recent developments of zinc oxide based photocatalyst in water treatment technology: a review, Water Res. 88 (2016)

428–448.
[30] G.A. Cerrón-Calle, A.J. Aranda-Aguirre, C. Luyo, S. Garcia-Segura, H. Alarcón, Photoelectrocatalytic decolorization of azo dyes with nano-composite oxide layers of ZnO nanorods decorated with Ag nanoparticles, Chemosphere 219 (2019) 296–304.
[31] S. Adhikari, A. Banerjee, N.K. Eswar, D. Sarkar, G. Madras, Photocatalytic inactivation of E. Coli by ZnO–Ag nanoparticles under solar radiation, RSC Adv. 5 (63) (2015) 51067–51077.
[32] Y. Liu, C. Xu, Z. Zhu, J. Lu, A.G. Manohari, Z. Shi, Self-assembled ZnO/Ag hollow spheres for effective photocatalysis and bacteriostasis, Mater. Res. Bull. 98 (2018) 64–69.
[33] C.R. Rajith Kumar, V.S. Betageri, G. Nagaraju, G.H. Pujar, H.S. Onkarappa, M.S. Latha, Synthesis of Core/Shell (ZnO/Ag) nanoparticles using calotropis gigantea and their applications in photocatalytic and antibacterial studies, J. Inorg. Organomet Polym. 30 (9) (2020) 3410–3417.
[34] T. Mahardika, N.A. Putri, A.E. Putri, V. Fauzia, L. Roza, I. Sugihartono, Y. Herbani, Rapid and low temperature synthesis of Ag nanoparticles on the ZnO nanorods for photocatalytic activity improvement, Results Phys. 13 (2019) 102209.
[35] R. Saravanan, N. Karthikeyan, V.K. Gupta, E. Thirumal, P. Thangadurai, V. Narayanan, A. Stephen, ZnO/Ag nanocomposite: An efficient catalyst for degradation studies of textile effluents under visible light, Mater. Sci. Eng. C 33 (4) (2013) 2235–2244.
[36] N.Q. Thang, A. Sabbah, L.-C. Chen, K.-H. Chen, L.V. Hai, C.M. Thi, P.V. Viet, Localized surface plasmonic resonance role of silver nanoparticles in the enhancement of long-chain hydrocarbons of the CO2 reduction over Ag-gC3N4/ZnO nanorods photocatalysts, Chem. Eng. Sci. 229 (2021) 116049.
[37] M.A. Qamar, S. Shahid, M. Javed, S. Iqbal, M. Sher, A. Bahadur, M.M. AL-Anazy, A. Laref, D. Li, Designing of highly active g-C_3N_4/Ni-ZnO photocatalyst nanocomposite for the disinfection and degradation of the organic dye under sunlight radiations, Colloids Surf. A Physicochem. Eng. Asp 614 (2021) 126176.
[38] Anise Akhundi, Alireza Badiei , Ghodsi Mohammadi Ziarani , Aziz Habibi-Yangjeh , Mario J. Muñoz-Batista , Rafael Luque, Graphitic carbon nitride-based photocatalysts: Toward efficient organic transformation for value-added chemicals production Molecular Catalysis Volume 488, June 2020, 110902 https://doi.org/10.1016/j.mcat.2020.110902.
[39] A. Akhundi, A. Habibi-Yangjeh, M. Abitorabi, S. Rahim Pouran, M. Abitorabi, S. Rahim Pouran, Review on photocatalytic conversion of carbon dioxide to value-added compounds and renewable fuels by graphitic carbon nitride-based photocatalysts, Catal. Rev. 61 (4) (2019) 595–628.
[40] A. Bahadur, S. Iqbal, M. Shoaib, A. Saeed, Electrochemical study of specially designed graphene-Fe_3O_4-polyaniline nanocomposite as a high-performance anode for lithium-ion battery, Dalton Trans. 47 (42) (2018) 15031–15037.
[41] Anise Akhundi, Alireza Zaker Moshfegh, Aziz Habibi-Yangjeh , and Mika Sillanpä, Simultaneous Dual-Functional Photocatalysis by g-C_3N_4-Based Nanostructures *ACS EST Engg.* 2022, 2, 564–585. https://doi.org/10.1021/acsestengg.1c00346.
[42] M.A. Qamar, M. Javed, S. Shahid, S. Iqbal, S.A. Abubshaitc, H.A. Abubshait, S.M. Ramay, A. Mahmood, H.M. Ghaithan, J. Environ, Chem. Eng. 9 (2021) 105534.
[43] I.M. Sundaram, S. Kalimuthu, G. Ponniah, Highly active ZnO modified g-C_3N_4 Nanocomposite for dye degradation under UV and Visible Light with enhanced stability and antimicrobial activity, Compos. Commun. 5 (2017) 64–71.
[44] T. Anusha, K.S. Bhavani, J.V. Shanmukha Kumar, P.K. Brahman, R.Y.A. Hassan, Fabrication of electrochemical immunosensor based on GCN-β-CD/Au nanocomposite for the monitoring of vitamin D deficiency, Bioelectrochemistry 143 (2022) 107935.
[45] Kampalapura Swamy, Chandrakantha, et al. "Microwave Hydrothermal Synthesis of Copper Induced ZnO/g-C_3N_4 Heterostructure With Efficient Photocatalytic Degradation Through S-scheme Mechanism." *Journal of Photochemistry and Photobiology A: Chemistry*, vol. 418, Elsevier BV, Sept. 2021, p. 113394. *Crossref*, https://doi.org/10.1016/j.jphotochem.2021.113394
[46] Y. Huang, Y.i. Tan, C. Feng, S. Wang, H. Wu, G. Zhang, Synthesis of CuO/g-C3N4 composites, and their application to voltammetric sensing of glucose and dopamine, Microchim Acta 186 (1) (2019), https://doi.org/10.1007/s00604-018-3120-z.
[47] N. Farooq, A.u. Rehman, A.M. Qureshi, Z.u. Rehman, A. Ahmad, M.K. Aslam, H.M.A. Javed, S. Hussain, M.A. Habila, N. AlMasoud, T.S. Alomar, Au@GO@g-C3N4 and Fe2O3 nanocomposite for efficient photocatalytic and electrochemical applications, Surf. Interfaces 26 (2021) 101399.
[48] X. Wei, H. Liu, T. Li, Z. Jiang, W. Hu, Q. Niu, J. Chen, Three-dimensional flower heterojunction g-C_3N_4/Ag/ZnO composed of ultrathin nanosheets with enhanced photocatalytic performance, J. Photochem. Photobiol. A Chem. 390 (2020) 112342.
[49] M. Sher, S.A. Khan, S. Shahid, M. Javed, M.A. Qamar, A. Chinnathambi, H.S. Almoallim, Synthesis of novel ternary hybrid g-C_3N_4@Ag-ZnO nanocomposite with Z-scheme enhanced solar light-driven methylene blue degradation and antibacterial activities, J. Environ. Chem. Eng. 9 (4) (2021) 105366.
[50] A. Stan, C. Munteanu, A.M. Musuc, R. Birjega, R. Ene, A. Ianculescu, I. Raut, L. Jecu, M. Badea Doni, E.M. Anghel, O. Carp, A general, eco-friendly synthesis procedure of self-assembled ZnO-based materials with multifunctional properties, Dalton Trans. 44 (17) (2015) 7844–7853.
[51] G. Sangeetha, S. Rajeshwari, R. Venckatesh, Green synthesis of zinc oxide nanoparticles by aloe barbadensis miller leaf extract: structure and optical properties, Mater. Res. Bull. 46 (12) (2011) 2560–2566.
[52] M. Bajpai, A. Pande, S.K. Tewari, D. Prakash, Phenolic contents and antioxidant activity of some food and medicinal plants, Int. J. Food Sci. Nutr. 56 (4) (2005) 287–291.
[53] D.V. Ponnuvelu, S.P. Suriyaraj, T. Vijayaraghavan, R. Selvakumar, B. Pullithadathail, Enhanced cell-wall damage mediated, antibacterial activity of core–shell ZnO@Ag heterojunction nanorods against Staphylococcus aureus and Pseudomonas aeruginosa, J. Mater. Sci.: Mater. Med. 26 (7) (2015).
[54] M. Sayed, J. Yu, G. Liu, M. Jaroniec, Mietek jaroniec non-noble plasmonic metal-based photocatalysts, Chem. Rev. 122 (11) (2022) 10484–10537.
[55] P. Xia, S. Cao, B. Zhu, M. Liu, M. Shi, J. Yu, Y. Zhang, Designing a 0D/2D S-Scheme Heterojunction over Polymeric Carbon Nitride for Visible-Light Photocatalytic Inactivation of Bacteria, Angew. Chem. Int. Ed. 59 (13) (2020) 5218–5225.
[56] Q. Xu, S. Wageh, A.A. Al-Ghamdi, X. Li, Design principle of S-scheme heterojunction photocatalyst Journal of Materials Science & Technology 124 (2022) 171–173.
[57] L. Zhang, J. Zhang, H. Yu, J. Yu, Emerging S-Scheme Photocatalyst, Adv. Mater. 34 (11) (2022) 2107668.